Islamic Azad University

Journal of

Optoelectronical Nanostructures

Summer 2022 / Vol.7, No. 3

Research Paper

Theoretical Assessment of Oxygen Adsorption Behavior onto Pristine, Be-and Ca-Doped Mg_{17} Nanoclusters

Mahmood Reza Dehghan[1], Sara Ahmadi*[,1], Zahrabatoul Mosapour Kotena[2,3]

[1] Department of Chemistry, Firoozabad Branch, Islamic Azad University, Firoozabad, Iran.
[2] Department of Chemistry, Faculty of Science, University of Malaya, 50603 Kuala Lumpur, Malaysia
[3] Department of Chemistry, Sharif University & Technology, P.O. Box 11365-9516, Tehran, Iran

Received: 5 Mar. 2022
Revised: 17 Jul. 2022
Accepted: 18 Aug. 2022
Published: 15 Sep 2022

Use your device to scan and read the article online

Keywords:
Adsorption, DFT, Electronic properties, Magnesium cluster, Oxygen.

Abstract:
Herein, the density functional theory (DFT) approach was used to investigate the behavior of oxygen during the adsorption over the magnesium nanoclusters $Mg_{16}M$ (M=Be, Mg, and, Ca). The electronic properties of $Mg_{16}M$ were remarkably Under the influence of absorption of the first and second O_2 molecules. NBO analysis showed charge transfer from nanoclusters to adsorbed O_2 molecules. According to E_{ads} and ΔH a thermodynamically desirable chemisorption process was foretoken. The negative values of ΔG are a witness to spontaneous adsorption. The DFT calculations show that the adsorption of the second oxygen is energetic more desirable than the first molecule. The $Mg_{16}Ca—O_2$ complex with the minimum bond length and maximum E_{ads} showed the strongest uni and di-molecular O_2 adsorption.

Citation: Mahmood Reza Dehghan, Sara Ahmadi, Zahrabatoul Mosapour Kotena. Theoretical assessment of oxygen adsorption behavior onto pristine, Be-and Ca-doped Mg_{17} nanoclusters. **Journal of Optoelectronical Nanostructures. 2022; 7 (3): 1- 22. DOI: 10.30495/JOPN.2022.29515.1245**

***Corresponding author:** Sara Ahmadi
Address: Department of Chemistry, Firoozabad Branch, Islamic Azad University, Firoozabad, Iran. **Tell:** +98-7138729701 **Email:** s.ahmadi@iauf.ac.ir

1. INTRODUCTION

Oxygen (O_2) is an active component of the atmosphere, which is the third most abundant element in the world after hydrogen and helium [1]. This diatomic molecule makes up 20.94% of the volume of the Earth's atmosphere [2]. Oxygen is needed in cells for aerobic respiration [3]. It can be used as a disinfectant to kill some anaerobic bacteria [4]. As the second largest industrial gas in the manufacture of steel and other processes of refining and manufacturing of metals, in chemicals, pharmaceuticals, oil processing, glass, ceramics, and paper production has numerous applications [5, 6]. The classical Winkler titration [7], electroanalytical [8], pressure-based [9], and optical methods [10] are several of popular methods for sensing oxygen gas which is very sophisticated. Therefore, many researchers are interested in finding a portable, rapid, and susceptible sensor for the retrieval and adsorption of oxygen gas. Recently, metal nanoclusters used as chemical sensors because of high surface-to-volume ratio, which is preferable to regular micro-detectors [11, 12].

In recent decades, nanomaterials have been identified as one of the most significant research subjects [13-15]. Improvements in the synthesis and properties of metal nanoclusters have led to the rapid development, and wide applications of these substances especially as catalytic agents, diagnosis of cancer, molecular electronics, and photonics of these materials [16-19]. Nanoclusters of second row metals with electron-filled layers show specific figure of the van der Waals bond among atoms [20]. Among divalent metal nanoclusters, magnesium nanoclusters have attractive attributes, such as low dielectric constant, high thermal conductivity, and oxidation resistance [21-24]. These properties of Mg atom have led to different usages like superconductivity [25], hydrogen storage [26, 27], nano-materials [28, 29], and biomedical [30].

The structure and electronic properties of magnesium nanoclusters have been studied through different theoretical methods. [31-36]. According to Xia et al., [35] the neutral magnesium nanoclusters of $Mg_{16}M$ are composed of an octagon frame (8-MR) at the center and two square frames (4-MRs) at the top and down are the most stable structures (Fig. 1).

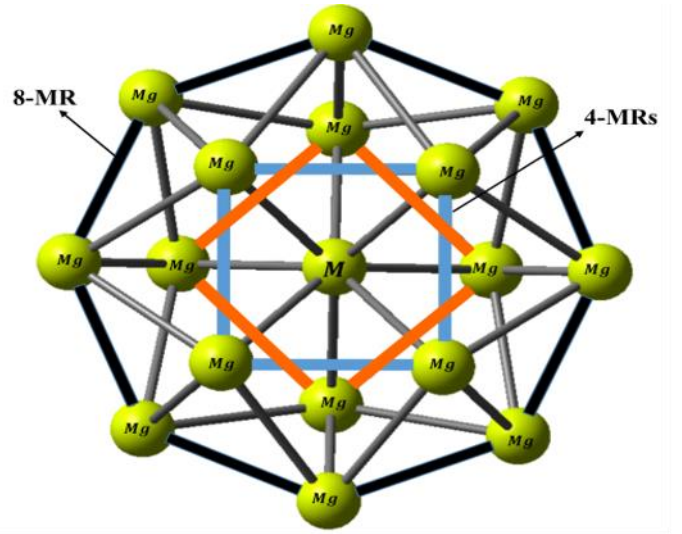

Fig. 1 The structure of Mg_{17} nanoclusters,

Oxygen adsorption subject on different nanostructures was studied theoretically and experimentally [37-40]. Tielens et al. studied the adsorption properties of O_2 molecule on the gold, gold/platinum, and platinum using periodic DFT calculations [41]. Oxygen adsorption on single-layer graphene was studied by Jin Yong Lee et al. using DFT method [42]. Herein, we probe the probability of the oxygen adsorption over the $Mg_{16}M$ (M=*Be*, *Mg*, and, *Ca*) using DFT calculations in the gas phase. DFT is a powerful and trustworthy method to study the metal nanocluster properties [36, 43-54]. The amount of the charge transfers between the O_2 molecule and $Mg_{16}M$ was evaluated by natural bond orbital (NBO) analysis [55]. The quiddity of the interactions was determined through the atoms in molecules (AIM) approach by AIM2000 software [56].

2. THEORETICAL METHODS

The modeling and optimization of the O_2 molecule, $Mg_{16}M$; (M=*Be*, *Mg*, and, *Ca*) nanoclusters, and studied complexes (uni- and di-oxygen adsorbed on the surface of $Mg_{16}M$) has been explained in our previous research [36, 49]. The CAM-B3LYP [47] with excellent capability which led to a long-range correction effect [57] and 6-311+g(d) basis set was applied to optimize the investigated systems in the gas phase using the Gaussian 09 package [58-59].

3. RESULTS and DISCUSSION

3.1 Geometry Optimization

The structure of neutral $Mg_{16}M$; (M=Be, Mg, and Ca) centered on Be, Mg, and Ca are optimized at the CAM-B3LYP/6-311+g(d) level of theory in the gas phase. Table 1 illustrate the obtained bond lengths and angles of $Mg_{16}M$. The obtained bond lengths are in the domain of relevant amount mentioned in Ref [62] and [63]. Obviously, bond lengths and angles are impressed by the central atom (M) in both 4-MR and 8-MR frames. The average bond for 4-MR frames increases with the size of the central atom, while the length of the 8-MR framework has an inverse design. Moreover, the average bond length of $Mg_{16}Mg$—O_2 complexes in both 4-MR and 8-MR frameworks changed significantly with the first adsorption of O_2 molecule except for $Mg_{16}Mg$—O_2.

Table 1 The average bond lengths in (Å) and bond angles in (°) of $Mg_{16}M$;(*M=Be, Mg,* and, *Ca*) before and after the first O_2 molecule adsorption in 4-MRs and 8-MR frames.

Nanoclusters	Metal ring frame	Bond lengths		Bond angles	
		Before the first adsorption	After the first adsorption	Before the first adsorption	After the first adsorption
$Mg_{16}Be$	8-MR	3.12	3.20	115.44	116.63
Mg_{17}		3.04	3.04	116.39	119.34
$Mg_{16}Ca$		2.95	3.25	112.76	128.21
$Mg_{16}Be$	4-MRs	2.92	3.06	89.99	90.92
Mg_{17}		3.05	3.23	90.01	90.87
$Mg_{16}Ca$		3.27	3.55	89.99	91.52

3.2 The Uni- and di-molecular Adsorption of O_2 over the $Mg_{16}M$ Nanoclusters

The adsorption behavior of the oxygen over the surface of different nanoclusters was examined by the interaction. The values of E_{ad}, E_{bind}, and E_{def} were calculated based on the following equations [64] Where *n* shows the number of O_2.

$$Mg_{16}M + nX \rightarrow Mg_{16}M \ldots X_n \qquad M = Be, Mg, Ca \qquad X = O_2 \qquad n = 1,2$$

$$E_{ad} = E_{Mg_{16}M \ldots X_n} - (E_{Mg_{16}M} + nE_X) \tag{1}$$

$$E_{bind} = E_{Mg_{16}M \ldots X_n} - (E_{Mg_{16}M\ in\ complex} + nE_{X\ in\ complex}) \tag{2}$$

$$E_{def} = E_{ad} - E_{bind} \tag{3}$$

3.2.1 Uni-molecular Adsorption

According to Table 2 in both 8-MR and 4-MRs frames, the distance between the $Mg_{16}M$ nanocluster and the first adsorbed O_2 molecule decreases by increasing the size of the central atom. Hence, the 4-MRs and 8-MR positions of the $Mg_{16}Ca$—O_2 complex have smaller bond distances (8-MR=1.89 and 4-MRs=1.91(Å)) compared to 4-MRs and 8-MR positions of the other complexes. The negative E_{ad} for 4-MRs and 8-MR frames of $Mg_{16}Be$—O_2 (-136.5801, -135.6389), Mg_{17}—O_2 (-138.7701, -134.9508), and $Mg_{16}Ca$—O_2 (-289.3990, -284.5090) all in kcal.mol-1, indicated a potent interaction among O_2 and different nanoclusters which revealed a chemisorption manner. The comparison between the adsorption energy values of 4-MRs and 8-MR frames in each nanocluster demonstrated that the 4-MRs frames are more desirable for O_2 adsorption than the 8-MR frame.

Table 2 The calculated binding distance (d), (E_{ad}), (E_{bind}), (E_{def}) (kcal/mol), and (E_{opt}) (a.u.) for O_2 adsorption over the $Mg_{16}Be$, $Mg_{16}Mg$ and $Mg_{16}Ca$ at the CAM-B3LYP/6-311+g(d) level of theory.

Complexes	Metal ring frame	d(Å)	E_{ad}	E_{bind}	E_{def}	E_{opt}
$Mg_{16}Be$—O_2	8 – MR	2.04	-135.6389	-189.6901	+54.0512	-3366.4761
$Mg_{16}Mg$—O_2		2.01	-134.9508	-201.3612	+66.4101	-3551.8447
$Mg_{16}Ca$—O_2		1.89	-284.5090	-521.9301	+237.4211	-4029.5781
$Mg_{16}Be$—O_2	4-MRs	2.03	-136.5801	-188.8211	+52.2410	-3366.4776
$Mg_{16}Mg$—O_2		1.98	-138.7701	-195.0214	+56.2513	-3551.8508
$Mg_{16}Ca$—O_2		1.91	-289.3990	-520.6121	+231.2131	-4029.5859
$Mg_{16}BeO_2$—O_2		1.94	-395.5008	-528.0021	+132.5013	-3517.1534
$Mg_{16}MgO_2$—O_2		1.93	-544.6302	-679.9513	+135.3211	-3702.7609
$Mg_{16}CaO_2$—O_2		1.89	-568.8921	-1046.6022	+477.7101	-4180.2945

As a result, the $Mg_{16}Ca$—O_2 has the most tendency to adsorb the first O_2 molecule. According to Eq. (1), the $E_{ad} < 0$ illustrates the stability of the obtained complex and the $E_{ad} > 0$ is related to the local minimum which shows the existence of a barrier during the adsorption. The E_{ad} includes the share of binding energy (E_{bind}) and deformation (E_{def}), both of which happen within the adsorption process [64]. The E_{def} values of the optimized $Mg_{16}M$—O_2 (M=*Be*, *Mg*, and, *Ca*) complexes are positive and vary according to the size of the middle atom

from a minority +52.24 to a utmost of +237.42 kcal/mol, for $Mg_{16}Be—O_2$ and $Mg_{16}Ca—O_2$ respectively. This indicates strong adsorption of the first O_2 molecule on the surface of studied nanoclusters. The chemical adsorption of the first O_2 molecule alters the electronic arrangement of the nanocluster, which in turn may break or weaken some of the bonds in nanocluster. Fig. 2 illustrates the uni- and di-molecular adsorption on the 4-MR frame for different nanoclusters. It is clear that during the uni- molecular O_2 adsorption on Mg_{17} and $Mg_{16}Be$ nanoclusters, the molecular structure of O_2 is preserved. The (O=O) bond is broken in $Mg_{16}Ca$ nanocluster and each oxygen atom adsorbs on different *Mg* atom of the nanocluster. According to the NBO results, the high charge transfer value (3.85914 e) was observed for the adsorption of the first oxygen on the surface of $Mg_{16}Ca$ nanocluster for 4-MR frame, which creates the highest interaction energy between the three nanoclusters [65-67]. Moreover, the calculated NBO charges illustrate the highest agglomeration of negative charge on the central M atom for each nanocluster (Table S6). The electron density depletion (EDD) map shows a Dense electronic cloud around the Mg—O, which represents oxygen adsorption over the nanoclusters (Fig. S1).

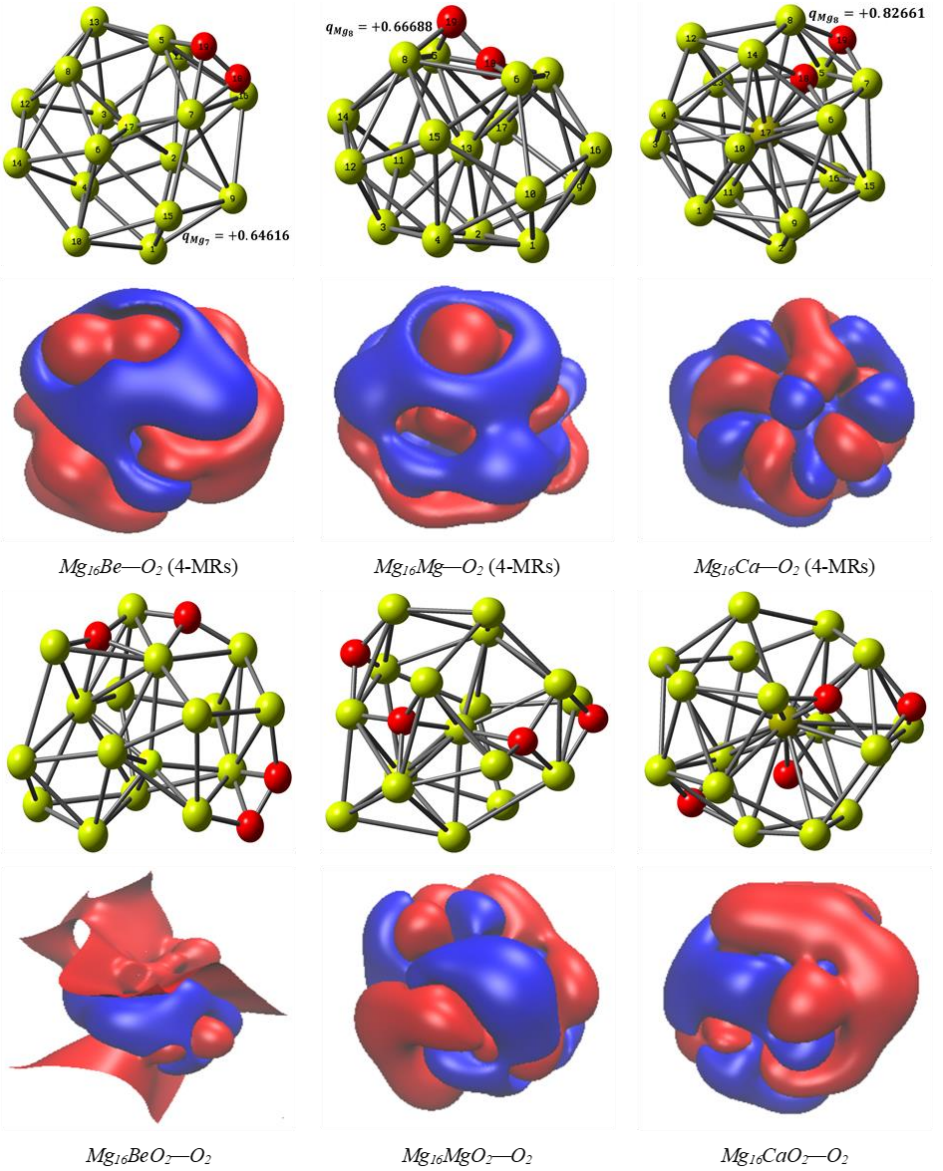

Fig. 2 The optimized structures of the uni and di-molecular adsorption complexes of $Mg_{16}M—O_2$ and $Mg_{16}MO_2—O_2$, *(M=Be, Mg, and, Ca)* at CAM-B3LYP/6-311+G(d) level of theory along with their corresponding EDD maps (0.001 au). In the EDD maps, the electron density depletion and accumulation sites are displayed in blue and red, respectively. *q* is the charge of the most positive atoms after the adsorption of the first O_2

molecule. The charge values of different *Mg* atoms are tabulated in Supplementary Table S7.

3.2.2 Di-molecular Adsorption

Table 2 indicate the 4-MRs frames are more stable than the 8-MR frame for three nanoclusters. Therefore, the second O_2 molecule was added to the most positive magnesium atom of the 4-MRs frames of each nanocluster. According to Table 2, the highest adsorption energy (-568.89 kcal/mol) was related to the $Mg_{16}CaO_2$—O_2 complex. Hence, $Mg_{16}Ca$ nanocluster shows the greatest tendency for di-molecular adsorption of O_2 molecule. Addition of the second oxygen is accompanied by the breaking of the (O=O) bond in $Mg_{16}BeO_2$—O_2, $Mg_{16}MgO_2$—O_2, and $Mg_{16}CaO_2$—O_2 complexes, which is the reason for the large deformation energies. Based on the NBO analysis, it appears that the large transfer charge of 3.56284 e from $Mg_{16}Ca$—O_2 complex to the O_2 molecule causes the $Mg_{16}CaO_2$—O_2 becomes the most stable di-molecular adsorbed complex.

3.3 Atoms in Molecules (AIM) Analysis

Bader's theory of atoms in molecules (AIM) is a powerful method to study the nature of the interactions [64] via parameters, such as electron density, $\rho_{(r)}$ and the Laplacian of the electron density, $\nabla^2{}_{\rho_{(r)}}$, which are computed at the bond critical point (BCP). For all studied complexes, the Laplacian of the total electron densities at BCPs of *Mg—O* are positive and reveal the electronic charges are depleted in the interatomic path, which is characteristic of the closed-shell interactions. The interaction behavior can be classified as a function of $H_{(r)}$ and the Laplacian of the electron density at BCP [68]. For strong interaction ($\nabla^2{}_{\rho_{(r)}} < 0$ and $H_{(r)} < 0$), the covalent character is established; for medium strength ($\nabla^2{}_{\rho_{(r)}} > 0$ and $H_{(r)} < 0$), the partially covalent character is defined; and weak ones with $\nabla^2{}_{\rho_{(r)}} > 0$ and $H_{(r)} > 0$ are mainly electrostatic interaction. As such, the interactions between all studied complexes have an electrostatic character in nature due to the positive values of $\nabla^2{}_{\rho_{(r)}}$ and $H_{(r)}$.

Table 3 reveals among the uni- and di-molecular adsorption complexes, $Mg_{16}Ca$—O_2 and $Mg_{16}CaO_2$—O_2 have the smallest intermolecular distances and highest electron density (with positive values). Furthermore, electron density analysis shows that the electron density in BCP enhances with the enhancement of the interaction energy.

Table 3 The electron density $\rho_{(r)}$, Laplacian of the electron density $\nabla^2{}_{\rho_{(r)}}$, for the Mg—O, at the bond critical points (BCPs); $G_{(r)}$, $V_{(r)}$, and $H_{(r)}$ at the CAM-B3LYP/6-311+G(d) level of theory.

uni-molecular adsorption of O_2 molecule						
Complexes	Metal ring Frame	$\rho_{(r)}$	$\nabla^2{}_{\rho_{(r)}}$	$G_{(r)}$	$V_{(r)}$	$H_{(r)}$
$Mg_{16}Be—O_2$	(8-MR)	0.0503	0.3804	0.0833	0.0715	0.1548
$Mg_{16}Mg—O_2$		0.0468	0.3583	0.0781	0.0667	0.1448
$Mg_{16}Ca—O_2$		0.0524	0.4064	0.0897	0.0778	0.1676
$Mg_{16}Be—O_2$	(4-MRs)	0.0504	0.3694	0.0815	0.0706	0.1521
$Mg_{16}Mg—O_2$		0.0437	0.3078	0.0673	0.0578	0.1251
$Mg_{16}Ca—O_2$		0.0573	0.4624	0.1026	0.0896	0.1923
di-molecular adsorption of O_2 molecule						
Complexes		$\rho_{(r)}$	$\nabla^2{}_{\rho_{(r)}}$	$G_{(r)}$	$V_{(r)}$	$H_{(r)}$
$Mg_{16}BeO_2—O_2$		0.0574	0.4644	0.1029	0.0897	0.1927
$Mg_{16}MgO_2—O_2$		0.0589	0.4795	0.1066	0.0934	0.2000
$Mg_{16}CaO_2—O_2$		0.0590	0.4796	0.1067	0.0935	0.2003

3.4. Electronic properties

The HOMO and LUMO values indicate the ability to donate and receive electrons, respectively [68]. The molecular reactivity and assessment of the sensibility of the studied nanoclusters regarding the oxygen molecule were measured by calculating the transition energy from HOMO to LUMO (E_{gap}). Table 4 illustrates the electronical properties for the studied complexes.

Table 4 summarizes the variation of the electronic properties of three nanoclusters and their complexes (uni- and di-molecular oxygen adsorbed) by replacing the central *Mg* atom in $Mg_{16}Mg$ with the *Ca* and *Be* atoms. It clearly shows that the energy gap of $Mg_{16}Mg$ varies from 2.5960 eV to 1.9484 eV and 3.0177 eV for $Mg_{16}Ca$ and $Mg_{16}Be$ respectively, which proves the electronic behavior of the $Mg_{16}M$ are susceptible to the central atom. On the other hand, Table 4 shows the (E_{gap}) values for uni-molecular (both 4-MR and 8-MR positions) and di-molecular O_2 adsorption over the $Mg_{16}M$ (M = *Mg* and *Ca*) increased incomparison to their pure nanoclusters, leading to more stability for uni- and di-molecular O_2 adsorption complexes of $Mg_{16}Mg$ and $Mg_{16}Ca$. Whilst, the uni-molecular (both 4-MR and 8-MR positions) and di-molecular O_2 adsorption upon the $Mg_{16}Be$ cause a decrease in the HOMO–LUMO from 3.0177 eV to 2.8409 eV and 2.7647 eV for 8-MR and 4-MR of $Mg_{16}Be—O_2$, respectively,

and also to 2.9932 eV for $Mg_{16}BeO_2$—O_2. This leads to instability for uni-and di-molecular adsorption of O_2 over the $Mg_{16}Be$. As a result, the uni-molecular and di-molecule adsorption of O_2 on the $Mg_{16}Be$ is associated with a decrease in gap energy and chemical hardness, so we expect the reactivity of these compounds to increase and their stability to decrease (Table 4) [69-71].

The chemical reactivity of the $Mg_{16}M$;(M=*Be*, *Mg*, and, *Ca*) can be specified according to the energy gap. Table 4, shows the $Mg_{16}Ca$ has less energy gap (1.9484 eV), less stability, and high chemical reactivity compared to the $Mg_{16}Mg$ (2.5960 eV) and $Mg_{16}Be$ (3.0177eV) nanoclusters, leading to greater sensibility towards the oxygen.

Table 4 The energy of (ε_{HOMO}), LUMO (ε_{LUMO}), (E_{gap}), (μ), (η) and (χ) (all in eV) for the investigated systems, at the CAM-B3LYP/6-311+g (d).

Structure	Metal ring frame	ε_{HOMO}	ε_{LUMO}	E_{gap}	ΔE_{gap}%	μ	η	χ
O_2		-9.0742	-3.5610	5.5132	—	-6.3204	2.7577	6.3204
$Mg_{16}Be$		-4.6749	-1.6572	3.0177	—	-3.1682	1.5089	3.1682
$Mg_{16}Mg$		-4.4599	-1.8639	2.5960	—	-3.1633	1.2981	3.1633
$Mg_{16}Ca$		-4.0518	-2.1034	1.9484	—	-3.0801	0.9742	3.0801
$Mg_{16}Be$—O_2	(8-MR)	-4.5307	-1.6898	2.8409	-5.86	-3.1093	1.4197	3.1093
$Mg_{16}Mg$—O_2		-4.5307	-1.8939	2.6368	+1.57	-3.2122	1.3193	3.2122
$Mg_{16}Ca$—O_2		-4.2504	-1.6762	2.5742	+32.12	-2.9640	1.2864	2.9640
$Mg_{16}Be$—O_2	(4-MRs)	-4.6123	-1.8476	2.7647	-8.38	-3.2311	1.3823	3.2311
$Mg_{16}Mg$—O_2		-4.6205	-1.8286	2.7919	+7.55	-3.2247	1.3966	3.2247
$Mg_{16}Ca$—O_2		-4.3946	-1.6572	2.7374	+40.50	-3.0279	1.3689	3.0279
$Mg_{16}BeO_2$—O_2		-4.6776	-1.6844	2.9932	-0.81	-3.1826	1.4963	3.1826
$Mg_{16}MgO_2$—O_2		-4.3375	-1.6517	2.6858	+3.46	-2.9952	1.3423	2.9952
$Mg_{16}CaO_2$—O_2		-4.3348	-1.6218	2.7130	+39.25	-2.9786	1.3565	2.9786

The chemical hardness is the resistance to changing the electronic configuration, while the electrochemical potential indicates a tendency to escape the electron cloud [72-74]. It appears that in various complexes, there is a reduction in chemical hardness with enhancing the size of the middle atom. Hereupon, the $Mg_{16}Ca$ nanocluster shows the most reactivity. As a result, the uni- and di-molecular adsorbed complexes of $Mg_{16}Ca$—O_2 (4-MRs and 8-MR) and $Mg_{16}CaO_2$—O_2 have high stability and low chemical reactivity in comparison to other complexes. On the other hand, in comparison between the 4-MRs and 8-MR frames of $Mg_{16}Ca$—O_2, the 4-MRs frame has a larger energy gap percent

(+40.50%) which represents high stability and low chemical reactivity. Comparing the ε_{HOMO} and ε_{LUMO} of the $Mg_{16}Ca$ with $Mg_{16}Ca—O_2$ represented that the ε_{HOMO} of the $Mg_{16}Ca$ was reduced from -4.0518 to -4.2504 eV and -4.3946 eV for the 8-MR and 4-RMs frames, respectively. Whereas, the ε_{LUMO} of the $Mg_{16}Ca$ was enhanced from -2.1034 to -1.6762 eV and -1.6572 eV for 8-MR and 4-MRs frames, respectively. In addition, the $\Delta E_{gap}\%$ (the percent of the nanoclusters band gap variations during the adsorption of O_2 molecule), has high values for the 8-MR frame (i.e; +32.12%) and 4-MRs frames (i.e; +40.50%) of the $Mg_{16}Ca$ nanocluster. Hence, the HOMO and LUMO level energies for the $Mg_{16}Ca$ nanocluster are remarkably under the influence of O2 molecule absorption. Resultantly, the O_2 can be detected by the $Mg_{16}Ca$ nanocluster.

$$N = A\,T^{3/2}\exp(-E_{gap}/2kT) \quad (4)$$

There is an exponential reduction between the electrical conductivity of the $Mg_{16}Ca$ nanocluster and the enhancement of the E_{gap}. This variation can be transformed into an electrical signal, which assists identify oxygen molecules.
Following, to inquire about the effects of the adsorption of oxygen on the electronic properties of the investigated complexes, the (DOSs) of these complexes have been summerised in Figures 3 and S3. The DOS plots determined, during the adsorption of the first and second oxygen molecule on the $Mg_{16}Ca$ nanoclusters ($Mg_{16}Ca—O_2$; 4-MRs and 8-MR and $Mg_{16}CaO_2—O_2$) as well as for $Mg_{16}Mg—O_2$; at 4-MRs and 8-MR, the conductivity levels moved toward higher energies compared to the energies of pristine nanoclusters.

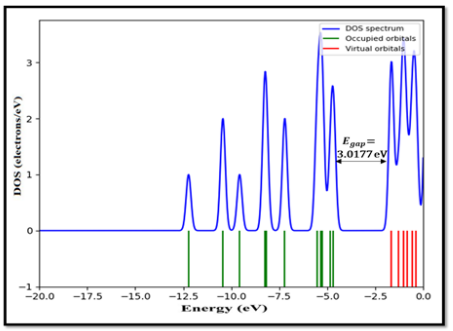

a) $Mg_{16}Be$ nanocluster

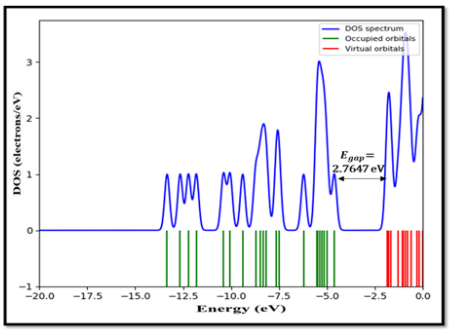

b) $Mg_{16}Be$—O_2 (4-MRs)

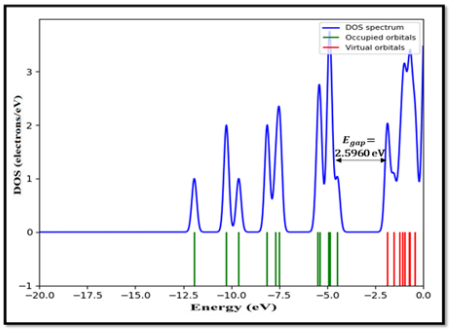

c) $Mg_{16}Mg$ nanocluster

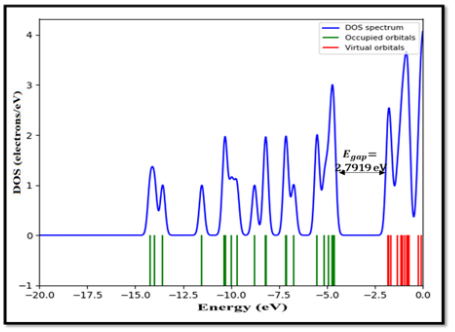

d) $Mg_{16}Mg$—O_2 (4-MRs)

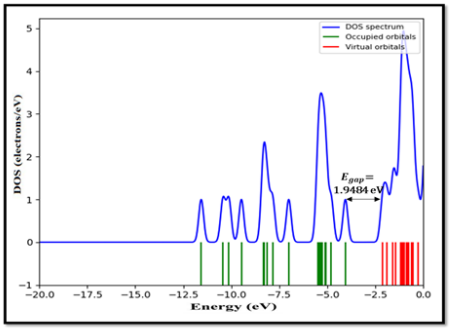

e) $Mg_{16}Ca$ nanocluster

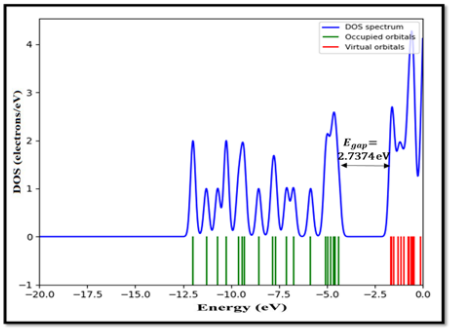

f) $Mg_{16}Ca$—O_2 (4-MRs)

Fig. 3 The representation of the electronic density of states (DOS) for adsorbed complexes. The E_{gap} shows the HOMO–LUMO energy gap.

3.5 Thermodynamic parameters

Table 5 shows the thermodynamic parameters calculated based on equation (5) at 298 K and 1 atmosphere.

$$\Delta X^{\circ} = X\,(Mg_{16}M \ldots O_2) - \left(\, X_{Mg_{16}M} + X_{O_2} \right) \quad X = H, G \tag{5}$$

Where $X_{Mg_{16}M\ldots O_2}$, $X_{Mg_{16}M}$ and X_{O_2} are thermodynamic parameters corresponding to the complex (nanocluster/O_2), nanocluster, and O_2 molecule respectively. The $\Delta H^{\circ} < 0$ for uni- and di-molecular oxygen adsorption indicated an exothermic reaction. According to Table 5, the ΔH° values for the first adsorbed oxygen over the 4-MRs frames are lower than the 8-MR positions in the three nanoclusters of $Mg_{16}Be$, $Mg_{16}Mg$, and $Mg_{16}Ca$. The of ΔH° values of the uni- and di-molecular adsorption of O_2 represent more stable adsorption for the second oxygen molecule on the 4-MRs frames. The negative values of $T\Delta S^{\circ}$ explain an entropy decrement through the adsorption process.

Table 5 The calculated thermodynamic properties (ΔH°, $T\Delta S^{\circ}$ and ΔG° all in kcal/mol) for studied complexes, at the CAM-B3LYP/6-311+g(d) approach.

Structure	Metal ring frame	ΔH°	ΔG°	$T\Delta S^{\circ}$
$Mg_{16}Be$—O_2		-134.9937	-123.4326	-11.5611
$Mg_{16}Mg$—O_2	(8-MR)	-134.5466	-124.8887	-9.6579
$Mg_{16}Ca$—O_2		-283.6930	-269.4781	-14.2149
$Mg_{16}Be$—O_2		-135.9236	-124.3106	-11.6130
$Mg_{16}Mg$—O_2	(4-MRs)	-138.5944	-127.3344	-11.2600
$Mg_{16}Ca$—O_2		-288.7097	-273.0525	-15.6572
$Mg_{16}BeO_2$—O_2		-393.9467	-370.9093	-23.0374
$Mg_{16}MgO_2$—O_2		-542.9176	-516.4079	-26.5097
$Mg_{16}CaO_2$—O_2		-567.2386	-538.4012	-28.8374

The negative values of ΔG° indicate a spontaneous and thermodynamically desirable adsorption process which results in an increment of the oxygen storage. Fig. S4 illustrates a good linear correlation between the E_{ad} and ΔH° of the studied complexes with the correlation coefficients of 0.9999. Interestingly, the ΔH^{0}_{ads} decreases with an increment of the radius of the central atom.

4.CONCLUSION

The adsorption of uni- and di-oxygen molecules on the surface of $Mg_{16}M$ (M=*Be*, *Mg*, and, *Ca*) was studied using the CAM-B3LYP/6-311+g(d) method. The negative values of the adsorption energies and thermodynamics properties (ΔH°, ΔG°) anticipate a spontaneous desirable adsorption process for investigated systems. The $Mg_{16}Ca$ nanocluster represents the most uni-molecular adsorption energy at the 4-MRs frame which leads to a significant charge transfer of 3.85914 e from nanocluster to O_2 molecule. Moreover, during the chemical adsorption of the O_2 molecule, the molecular structure of the second oxygen is broken down. Interestingly, the di-molecular adsorption of the oxygen is more desirable than the uni-molecular adsorption. The NBO analysis proved that in the studied complexes, the nanocluster is an electron-donating and the oxygen molecule is the electron acceptor. We foretaste that replacing the central magnesium atom with a divalent metal with a larger radius than magnesium could enhance the sensitivity of the $Mg_{16}M$ to be used as an O_2 gas sensor.

CONFLICT OF INTEREST

The authors state that publication of this manuscript does not involve any conflicts of interest.

REFERENCES

[1] W.M. Haynes, *CRC handbook of chemistry and physics*, 95 ed., CRC press, 2014. Available: https://doi.org/10.1201/b17118

[2] A.E. Galashev, *Molecular-dynamic modeling of ultradisperse water in the earth atmosphere*. High Temp., 48 (4) (2010) 518-526. Available: https://doi.org/10.1134/S0018151X10040097

[3] K.M. Manoj, V. Soman, V.D. Jacob, A. Parashar, D.A. Gideon, M. Kumar, A. Manekkathodi, S. Ramasamy, K. Pakshirajan, N.M. Bazhin, *Chemiosmotic and murburn explanations for aerobic respiration: predictive capabilities, structure-function correlations and chemico-physical logic*. ARCH BIOCHEM BIOPHYS., 676 (2019) 108128. Available: https://doi.org/10.1016/j.abb.2019.108128

[4] R. Reed, *Solar inactivation of faecal bacteria in water: the critical role of oxygen, Lett.* Appl. Microbiol., 24 (4) (1997) 276-280. Available: https://doi.org/10.1046/j.1472-765X.1997.00130.x

[5] D.B. Papkovsky, G.V. Ponomarev, W. Trettnak, P. O'Leary, *Phosphorescent complexes of porphyrin ketones: optical properties and application to oxygen sensing*. Anal. Chem., 67 (22) (1995) 4112-4117. Available: https://doi.org/10.1021/ac00118a013

[6] W. Yang, H. Wang, X. Zhu, L. Lin, *Development and application of oxygen permeable membrane in selective oxidation of light alkanes*. J. Top. Catal., 35 (1-2) (2005) 155-167. Available: https://doi.org/10.1007/s11244-005-3820-6

[7] L.W. Winkler, *The determination of dissolved oxygen in water*. Berlin DeutChem Gas., 21 (1888) 2843-2855.

[8] K. Kinoshita, *Electrochemical oxygen technology*, John Wiley & Sons., vol. 30, 1992.

[9] R. Ramamoorthy, P. Dutta, S. Akbar, *Oxygen sensors: materials, methods, designs and applications*. J. Mater. Sci., 38 (21) (2003) 4271-4282. Available: https://doi.org/10.1023/A:1026370729205

[10] Y. Amao, *Probes and polymers for optical sensing of oxygen*. Microchim. Acta., 143 (1) (2003) 1-12. Available: https://doi.org/10.1007/s00604-003-0037-x

[11] N.L. Hadipour, A. Ahmadi Peyghan, H. Soleymanabadi, *Theoretical study on the Al-doped ZnO nanoclusters for CO chemical sensors*. J. Phys. Chem.

C., 119 (11) (2015) 6398-6404. Available: https://doi.org/10.1021/jp513019z

[12] E. Vessally, S.A. Siadati, A. Hosseinian, L. Edjlali, *Selective sensing of ozone and the chemically active gaseous species of the troposphere by using the C20 fullerene and graphene segment*. Talanta., 162 (2017) 505-510. Available: https://doi.org/10.1016/j.talanta.2016.10.010

[13] G. Aragay, F. Pino, A. Merkoçi, *Nanomaterials for sensing and destroying pesticides*. Chemical reviews., 112 (10) (2012) 5317-5338. Available: https://doi.org/10.1021/cr300020c

[14] S. Guo, S. Dong, *Graphene nanosheet: synthesis, molecular engineering, thin film, hybrids, and energy and analytical applications*. Chemical Society Reviews., 40 (5) (2011) 2644-2672. Available: https://doi.org/10.1039/c0cs00079e

[15] S. Guo, E. Wang, *Functional micro/nanostructures: simple synthesis and application in sensors, fuel cells, and gene delivery*. Accounts of Chemical Research., 44 (7) (2011) 491-500. Available: https://doi.org/10.1021/ar200001m

[16] M. Zhu, C.M. Aikens, F.J. Hollander, G.C. Schatz, R. Jin, *Correlating the crystal structure of a thiol-protected Au25 cluster and optical properties*. Journal of the American Chemical Society., 130 (18) (2008) 5883-5885. Available: https://doi.org/10.1021/ja801173r

[17] O. Varnavski, G. Ramakrishna, J. Kim, D. Lee, T. Goodson, *Critical size for the observation of quantum confinement in optically excited gold clusters*. Journal of the American Chemical Society, 132 (1) (2010) 16-17. Available: https://doi.org/10.1021/ja907984r

[18] S.H. Yau, O. Varnavski, T. Goodson III, *An ultrafast look at Au nanoclusters*. Accounts of chemical research., 46 (7) (2013) 1506-1516. Available: https://doi.org/10.1021/ar300280w

[19] P.D. Jadzinsky, G. Calero, C.J. Ackerson, D.A. Bushnell, R.D. Kornberg, *Structure of a thiol monolayer-protected gold nanoparticle at 1.1 Å resolution*. Science., 318 (5849) (2007) 430-433. Available: https://doi.org/10.1126/science.1148624

[20] J. Zheng, P.R. Nicovich, R.M. Dickson, *Highly fluorescent noble-metal quantum dots*. Annu. Rev. Phys. Chem., 58 (2007) 409-431. Available: https://doi.org/10.1146/annurev.physchem.58.032806.104546

[21] I. Heidari, S. De, S. Ghazi, S. Goedecker, D. Kanhere, *Growth and Structural Properties of Mg N (N= 10–56) Clusters: Density Functional Theory Study*. J. Phys. Chem A., 115 (44) (2011) 12307-12314. Available: https://doi.org/10.1021/jp204442e

[22] S. Janecek, E. Krotscheck, M. Liebrecht, R. Wahl, *Structure of Mg n and Mg n+ clusters up to n= 30*. Eur. Phys. J. D., 63 (3) (2011) 377-390. Available: https://doi.org/10.1140/epjd/e2011-10694-2

[23] A. Köhn, F. Weigend, R. Ahlrichs, *Theoretical study on clusters of magnesium*. Phys. Chem. Chem. Phys., 3 (5) (2001) 711-719. Available: https://doi.org/10.1039/b007869g

[24] A. Lyalin, I.A. Solov'yov, A.V. Solov'yov, W. Greiner, *Evolution of the electronic and ionic structure of Mg clusters with increase in cluster size*. Phys. Rev. A., 67 (6) (2003) 063203-063215. Available: https://doi.org/10.1103/PhysRevA.67.063203

[25] M. Monteverde, M. Nunez-Regueiro, N. Rogado, K. Regan, M. Hayward, T. He, S. Loureiro, R.J. Cava, *Pressure dependence of the superconducting transition temperature of magnesium diboride*. Science., 292 (5514) (2001) 75-77. Available: https://doi.org/10.1126/science.1059775

[26] S. Er, G.A. de Wijs, G. Brocks, *Tuning the hydrogen storage in magnesium alloys*. J. Phys. Chem. Lett., 1 (13) (2010) 1982-1986. Available: https://doi.org/10.1021/jz100386j

[27] R. Nevshupa, J.R. Ares, J.F. Fernández, A. del Campo, E. Roman, *Tribochemical decomposition of light ionic hydrides at room temperature*. J. Phys. Chem. Lett., 6 (14) (2015) 2780-2785. Available: https://doi.org/10.1021/acs.jpclett.5b00998

[28] G. Barcaro, R. Ferrando, A. Fortunelli, G. Rossi, *Exotic supported copt nanostructures: from clusters to wires*. J. Phys. Chem. Lett., 1 (1) (2009) 111-115. Available: https://doi.org/10.1021/jz900076m

[29] L.-Y. Chen, J.-Q. Xu, H. Choi, M. Pozuelo, X. Ma, S. Bhowmick, J.-M. Yang, S. Mathaudhu, X.-C. Li, *Processing and properties of magnesium containing a dense uniform dispersion of nanoparticles*. Nature., 528 (7583) (2015) 539-543. Available: https://doi.org/10.1038/nature16445

[30] J. Yoo, A. Aksimentiev, *Improved parametrization of Li+, Na+, K+, and Mg2+ ions for all-atom molecular dynamics simulations of nucleic acid systems*. J. Phys. Chem. Lett., 3 (1) (2011) 45-50. Available: https://doi.org/10.1021/jz201501a

[31] J. Akola, K. Rytkönen, M. Manninen, *Metallic evolution of small magnesium clusters*. Eur. Phys. J. D., 16 (1) (2001) 21-24. Available: https://doi.org/10.1007/s100530170051

[32] E.R. Davidson, R.F. Frey, *Density functional calculations for Mg n+ clusters*. J. Chem. Phys., 106 (6) (1997) 2331-2341. Available: https://doi.org/10.1063/1.473096

[33] X. Gong, Q. Zheng, Y.-z. He, *Electronic structures of magnesium clusters*, *Phys*. Lett. A., 181 (6) (1993) 459-464. Available: https://doi.org/10.1016/0375-9601(93)91150-4

[34] V. Kumar, R. Car, Structure, *growth, and bonding nature of Mg clusters*, *Phys*. Rev. B., 44 (15) (1991) 8243-8255. Available: https://doi.org/10.1103/PhysRevB.44.8243

[35] X. Xia, X. Kuang, C. Lu, Y. Jin, X. Xing, G. Merino, A. Hermann, *Deciphering the structural evolution and electronic properties of magnesium clusters: an aromatic homonuclear metal Mg17 cluster*. J. Phys. Chem. A., 120 (40) (2016) 7947-7954. Available: https://doi.org/10.1021/acs.jpca.6b07322

[36] M.R. Dehghan, S. Ahmadi, Z.M. Kotena, *Adsorption behaviors of carbon monoxide (CO) over aromatic magnesium nanoclusters: a DFT study*. Structural Chemistry., 32 (1) (2021) 1949-1960. Available: https://doi.org/10.1007/s11224-021-01770-6

[37] S. Zhuiykov, *In situ FTIR study of oxygen adsorption on nanostructured RuO 2 thin-film electrode*. Ionics., 15 (4) (2009) 507-512. Available: https://doi.org/10.1007/s11581-008-0294-0

[38] F. Gobal, R. Arab, M. Nahali, *A comparative DFT study of atomic and molecular oxygen adsorption on neutral and negatively charged PdxCu3− x (x= 0–3) nano-clusters*. Journal of Molecular Structure: THEOCHEM., 959 (1-3) (2010) 15-21. Available: https://doi.org/10.1016/j.theochem.2010.07.042

[39] S. Tan, Y. Ji, Y. Zhao, A. Zhao, B. Wang, J. Yang, J. Hou, *Molecular oxygen adsorption behaviors on the rutile TiO2 (110)-1× 1 surface: an in situ study with low-temperature scanning tunneling microscopy*. J. Am. Chem. Soc., 133 (6) (2011) 2002-2009. Available: https://doi.org/10.1021/ja110375n

[40] F. Tielens, J. Andrés, T.-D. Chau, T.V. de Bocarmé, N. Kruse, P. Geerlings, *Molecular oxygen adsorption on electropositive nano gold tips*. Chem. Phys. Lett., 421 (4-6) (2006) 433-438. Available: https://doi.org/10.1016/j.cplett.2006.02.006

[41] F. Tielens, J. Andrés, M. Van Brussel, C. Buess-Hermann, P. Geerlings, *DFT study of oxygen adsorption on modified nanostructured gold pyramids*. J. Phys. Chem. B., 109 (16) (2005) 7624-7630. Available: https://doi.org/10.1021/jp0501897

[42] B. Kang, H. Liu, J.Y. Lee, *Oxygen adsorption on single layer graphyne: a DFT study*. Phys. Chem. Chem. Phys., 16 (3) (2014) 974-980. Available: https://doi.org/10.1039/C3CP53237B

[43] H.A. Al-Abadleh, V. Grassian, *FT-IR study of water adsorption on aluminum oxide surfaces*. Langmuir., 19 (2) (2003) 341-347. Available: https://doi.org/10.1021/la026208a

[44] J.-K. Chen, S.-M. Yang, B.-H. Li, C.-H. Lin, S. Lee, *Fluorescence quenching investigation of methyl red adsorption on aluminum-based metal–organic frameworks*. Langmuir., 34 (4) (2018) 1441-1446. Available: https://doi.org/10.1021/acs.langmuir.7b04240

[45] X.-J. Kuang, X.-Q. Wang, G.-B. Liu, *A density functional study on the adsorption of hydrogen molecule onto small copper clusters*. J. Chem. Sci., 123 (5) (2011) 743-754. Available: https://doi.org/10.1007/s12039-011-0130-3

[46] Q.-M. Ma, Z. Xie, J. Wang, Y. Liu, Y.-C. Li, *Structures, binding energies and magnetic moments of small iron clusters: A study based on all-electron DFT*. Solid State Commun., 142 (1-2) (2007) 114-119. Available: https://doi.org/10.1016/j.ssc.2006.12.023

[47] R. Hussain, A.I. Hussain, S.A.S. Chatha, A. Mansha, K. Ayub, *Density functional theory study of geometric and electronic properties of full range of bimetallic AgnYm (n+ m= 10) clusters*. J. Alloys Compd., 705 (2017) 232-246. Available: https://doi.org/10.1016/j.jallcom.2017.02.008

[48] S.F. Matar, *DFT study of hydrogen instability and magnetovolume effects in CeNi*. Solid State Sci., 12 (1) (2010) 59-64. Available: https://doi.org/10.1016/j.solidstatesciences.2009.10.003

[49] M.R. Dehghan, S. Ahmadi, Z.M. Kotena, M. Niakousari, *A computational study of N2 adsorption on aromatic metal Mg16M;(M= Be, Mg, and Ca) nanoclusters*. Journal of Molecular Graphics and Modelling., 105 (2021) 107862. Available: https://doi.org/10.1016/j.jmgm.2021.107862

[50] M.R. Dehghan, S. Ahmadi, *Adsorption Behaviour of CO Molecule on Mg16M—O2 Nanostructures (M= Be, Mg, and Ca): A DFT Study*. Journal of Optoelectronical Nanostructures., 6 (1) (2021) 1-20. Available:https://dorl.net/dor/20.1001.1.24237361.2021.6.1.1.3

[51] S.J. Mousavi, *Ab-initio LSDA Study of the Electronic States of Nano Scale Layered LaCoO3/Mn Compound: Hubbard Parameter Optimization*. JOPN., 5 (4) (2020) 111-122. Available: https://dorl.net/dor/20.1001.1.24237361.2020.5.4.7.8

[52] H. Salehi, *Ab-initio study of Electronic, Optical, Dynamic and Thermoelectric properties of CuSbX2 (X= S, Se) compounds*. JOPN., 3 (2) (2018) 53-64. Available: https://dorl.net/dor/20.1001.1.24237361.2018.3.2.5.8

[53] M. Askaripour Lahiji, A. Abdolahzadeh Ziabari, *Ab–initio study of the electronic and optical traits of Na0. 5Bi0. 5TiO3 nanostructured thin film*. JOPN., 4 (3) (2019) 47-58. Available: https://dorl.net/dor/20.1001.1.24237361.2019.4.3.4.6

[54] S.J. Mousavi, *First–Principle Calculation of the Electronic and Optical Properties of Nanolayered ZnO Polymorphs by PBE and mBJ Density Functionals*. JOPN., 2 (4) (2017) 1-18. Available: https://dorl.net/dor/20.1001.1.24237361.2017.2.4.1.1

[55] F. Weinhold, C.R. Landis, *Natural bond orbitals and extensions of localized bonding concepts*. CHEM EDUC RES PRACT., 2 (2) (2001) 91-104. Available: https://doi.org/10.1039/B1RP90011K

[56] F. Biegler- König, J. Schönbohm, *Update of the AIM2000- program for atoms in molecules*. J. Comput. Chem., 23 (15) (2002) 1489-1494. Available: https://doi.org/10.1002/jcc.10085

[57] Y. Fu, T. Lu, Y. Xu, M. Li, Z. Wei, H. Liu, W. Lu, *Theoretical screening and design of SM315-based porphyrin dyes for highly efficient dye-sensitized solar cells with near-IR light harvesting*. Dyes Pigm., 155 (2018) 292-299. Available: https://doi.org/10.1016/j.dyepig.2018.03.045

[58] M. Frisch, G. Trucks, H.B. Schlegel, G. Scuseria, M. Robb, J. Cheeseman, G. Scalmani, V. Barone, B. Mennucci, G. Petersson, Gaussian 09, Revision B.01, (Gaussian, Inc., Wallingford, CT, 2009).

[59] S.F. Boys, F. Bernardi, *The calculation of small molecular interactions by the differences of separate total energies. Some procedures with reduced errors*. Mol. Phys., 19 (4) (1970) 553-566. Available: https://doi.org/10.1080/00268977000101561

[60] N.M. O'boyle, A.L. Tenderholt, K.M. Langner, *Cclib: a library for package- independent computational chemistry algorithms*. J. Comput. Chem., 29 (5) (2008) 839-845. Available: https://doi.org/10.1002/jcc.20823

[61] T. Lu, F. Chen, *Multiwfn: a multifunctional wavefunction analyzer*. J. Comput. Chem., 33 (5) (2012) 580-592. Available: https://doi.org/10.1002/jcc.22885

[62] K.-P. Huber, *Molecular spectra and molecular structure: IV. Constants of diatomic molecules*. Springer Science & Business Media., 2013.

[63] R.D. Johnson III, *NIST Computational Chemistry Comparison and Benchmark Database*. http://srdata. nist. gov/cccbdb. 2006. Available: http://cccbdb.nist.gov/

[64] M. Shahabi, H. Raissi, *Molecular dynamics simulation and quantum chemical studies on the investigation of aluminum nitride nanotube as phosgene gas sensor*. Journal of Inclusion Phenomena and Macrocyclic Chemistry., 86 (3-4) (2016) 305-322. Available: https://doi.org/10.1007/s10847-016-0664-6

[65] A. Hosseinian, E. Vessally, A. Bekhradnia, S. Ahmadi, P.D.K. Nezhad, *Interaction of α-cyano-4-hydroxycinnamic acid drug with inorganic BN nanocluster: A density functional study*. J Inorg Organomet Polym Mater., 28 (4) (2018) 1422-1431. Available: https://doi.org/10.1007/s10904-018-0778-y

[66] E. Vessally, F. Behmagham, B. Massuomi, A. Hosseinian, K. Nejati, *Selective detection of cyanogen halides by BN nanocluster: a DFT study*. J. Mol. Model., 23 (4) (2017) 1-9. Available:https://doi.org/10.1007/s00894-017-3312-1

[67] K. Nejati, A. Hosseinian, E. Vessally, A. Bekhradnia, L. Edjlali, *A comparative DFT study on the interaction of cathinone drug with BN nanotubes, nanocages, and nanosheets*. Appl. Surf. Sci., 422 (2017) 763-768. Available: https://doi.org/10.1016/j.apsusc.2017.06.082

[68] S. Ahmadi, V.M. Achari, H. Nguan, R. Hashim, *Atomistic simulation studies of the α/β-glucoside and galactoside in anhydrous bilayers: effect of the anomeric and epimeric configurations*. J. Mol. Model., 20 (3) (2014) 1-12. Available: https://doi.org/10.1007/s00894-014-2165-0

[69] Z. Zhou, R.G. Parr, *Activation hardness: new index for describing the orientation of electrophilic aromatic substitution*. J. Am. Chem. Soc., 112 (15) (1990) 5720-5724. Available: https://doi.org/10.1021/ja00171a007

[70] R.G. Pearson, *Absolute electronegativity and hardness: applications to organic chemistry*. J. Org. Chem., 54 (6) (1989) 1423-1430. Available: https://doi.org/10.1021/jo00267a034

[71] W. Faust, *Explosive molecular ionic crystals*. Science., 245 (4913) (1989) 37-42. Available: https://doi.org/10.1126/science.245.4913.37

[72] R.G. Parr, R.G. Pearson, *Absolute hardness: companion parameter to absolute electronegativity*. J. Am. Chem. Soc., 105 (26) (1983) 7512-7516. Available: https://doi.org/10.1021/ja00364a005

[73] R.G. Parr, P.K. Chattaraj, *Principle of maximum hardness*. J. Am. Chem. Soc., 113 (5) (1991) 1854-1855. Available: https://doi.org/10.1021/ja00005a072

[74] R.G. Pearson, *Absolute electronegativity and absolute hardness of Lewis acids and bases*. J. Am. Chem. Soc., 107 (24) (1985) 6801-6806. Available: https://doi.org/10.1021/ja00310a009